MICROWAVE APPLICATIONS OF PHOTONIC CRYSTALS

E. Ozbay, B. Temelkuran, and M. Bayindir

Abstract—We have demonstrated guiding and bending of electromagnetic (EM) waves in planar and coupled-cavity waveguides built around three-dimensional layer-by-layer photonic crystals. We observed full transmission of the EM waves through these waveguide structures. The dispersion relations obtained from the experiments were in good agreement with the predictions of our waveguide models. We also reported a resonant cavity enhanced (RCE) effect by placing microwave detectors in defect structures. A power enhancement factor of 3450 was measured for planar cavity structures. Similar defects were used to achieve highly directional patterns from monopole antennas.

1. INTRODUCTION

A decade ago, it was suggested that an artificially created periodic structure might result in a stop band for electromagnetic (EM) waves, where the propagation of the waves were inhibited in a certain range of frequencies in all directions [1, 2]. In analogy with electronic bandgaps

in semiconductors, these structures are called photonic band gap (PBG) materials or photonic crystals [3, 4].

The initial interest in this area came from the proposal to use photonic crystals to control spontaneous emission in photonic devices [1]. However, the technological challenges restricted most of the experimental demonstrations and relevant applications of these crystals to millimeter wave and microwave frequencies [5–8]. Recently, a three-dimensional (3D) photonic crystal with a band gap at optical frequencies was reported [9–11]. With this breakthrough, initally proposed applications like thresholdless semiconductor lasers [12] and single-mode light-emitting diodes [13, 14] became feasible.

One other important aspect of the photonic crystals is that, just like the donor or acceptor states in an electronic crystal, breaking the periodicity of the crystal results in localization of the EM field within the defect volume [15]. With these properties, photonic crystals are novel structures that can be used to control the behaviour of light. Very recently, the two-dimensional bandgap laser was demonstrated [16, 17]. The cavity consisted of one filled hole (a defect) in an otherwise periodic array of holes penetrating a light emitting, semiconducting film [16].

In this paper, we will present three important applications of photonic band gap materials: waveguides, detectors, and antennas. In the first part, we will demonstrate the propagation of the EM waves through a waveguide built around photonic crystals [7, 18, 19]. The second one is the detection of the EM wave, in which we will introduce a detector whose sensitivity and selectivity are significantly improved by using photonic crystals [6]. In the last section, we will show that the radiated field from a monopole antenna inserted within the defect volume of the photonic crystal is highly directional and enhanced [8].

2. THREE-DIMENSIONAL LAYER-BY-LAYER PHOTONIC CRYSTALS

In our experiments, we used a layer-by-layer structure [20, 21] which was constructed by using square-shaped alumina rods (0.32 cm × 0.32 cm × 15.25 cm) of refractive index 3.1 at microwave frequencies. The stacking sequence repeats every four layers, which has the equivalent geometry of a face centered tetragonal (fct) lattice, corresponding to a single unit cell in the stacking direction. The crystal has a center to center separation of 1.12 cm, with a dielectric filling ratio of ~ 0.29 [Fig. 1(a)]. The layer-by-layer photonic crystal is the first structure that was fabricated at optical frequencies [9–11].

We measured the transmission and reflection spectra of the structure by using a Hewlett-Packard 8510C network analyzer. Stan-
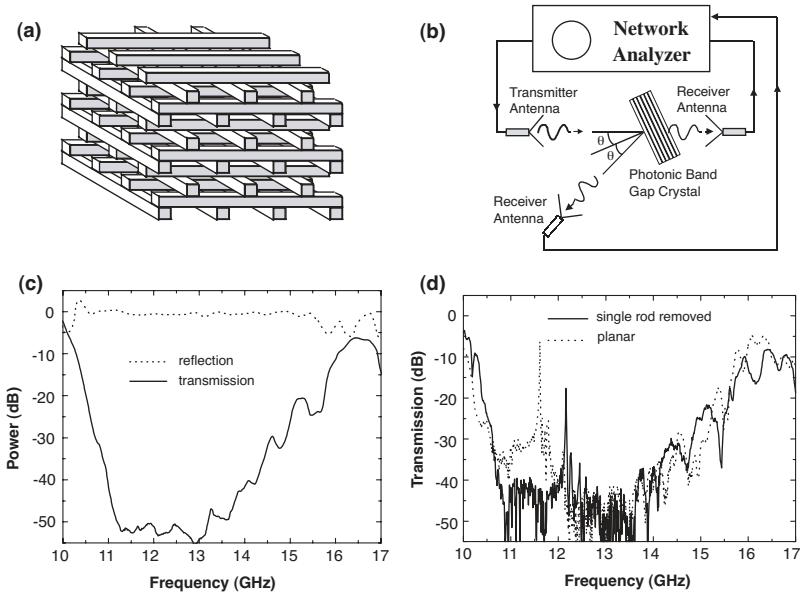
Figure 1. (a) Schematics of a three-dimensional layer-by-layer photonic crystal. (b) The experimental setup for measuring the transmission and reflection characteristics of the photonic crystal. (c) Transmission (solid line) and reflection (dotted line) profiles of 4-unit cell periodic structure along the stacking direction. (d) Transmission characteristics of a single rod removed (solid line) and planar (dotted line) defect structures.

dard gain horn antennas were used to transmit and receive the EM radiation [Fig. 1(b)]. Surroundings of the setup were covered with absorbers resulting in a sensitivity around 70 dB. Figure 1(c) shows the transmission (solid line) and reflection (dotted line) through a 4-unit cell crystal along the stacking direction. Almost all incident EM waves were reflected within the stop-band of the photonic crystal. The transmission is around −55 dB within the band gap, corresponding to 3.5 dB attenuation per layer. The transmission measurements performed at different angles and polarizations showed that the three-dimensional stop band, referred to as the photonic band gap, extends from 10.6 to 12.7 GHz, which agrees well with the expectations of the theory [22].

Breaking the periodicity of the crystal resulted in evanescent

modes within the PBG. We tested two types of such defect structures. Figure 1(d) (solid line) shows the transmission spectrum of a 16-layer (4-unit cell) crystal with a single rod missing from the 8th layer. The resonant frequency of the defect mode is at 12.16 GHz with a Q-factor (quality factor defined as center frequency divided by the peak's full width at half-maximum) is 1380. We also created planar defects by separating the 8th and 9th layers of a 16-layer crystal. The defect frequency, which can be tuned by changing the width of the air gap, appeared at 11.61 GHz for a separation of 8.6 mm [Fig. 1(d), dotted line], with a Q-factor of 1570 [23].

3. PHOTONIC CRYSTAL BASED WAVEGUIDES

3.1. Planar Waveguides

Photonic crystals provide a promising tool to control the flow of light in integrated optical devices [24, 25]. Therefore, there is great deal of interest in developing photonic crystal based waveguides where one can confine and efficiently guide the light around sharp corners [7, 18, 26–32].

The basic motivation in photonic crystal based waveguides arose when the following properties of the PBG materials, which are essential for many applications, were considered. First, photonic crystals have the property of reflecting the EM waves within the band gap frequencies in all directions. Second, defect structures in which the EM wave is trapped, can be created by breaking the periodicity of the crystal. Combining these two properties, an opening carved all through an otherwise-perfect crystal (which resembles a continuous defect structure), may serve as a waveguide. Once the EM wave is coupled inside the guide, the trapped wave, which has no where else to go, is guided through the opening inside the crystal. This guiding mechanism is superior to traditional waveguides which rely on total internal reflection of the EM waves. The serious leakage problem for the EM waves traveling around tight corners in a traditional waveguide can be solved by using a photonic crystal based waveguide, and smaller scale optoelectronic integrated circuits can be successfully built [11, 33].

Figure 2(a) shows the schematics of the measurement set-up that was used in our experiments. The horn antennas kept 5 cm away from the crystal. We measured the transmission-phase and transmission-amplitude properties of the two different waveguide structures, namely a parallel-plate and an L-shape. We constructed the parallel-plate type waveguide by using two separate 3-unit cells thick layer-by-layer photonic crystals. The crystals were brought together along the
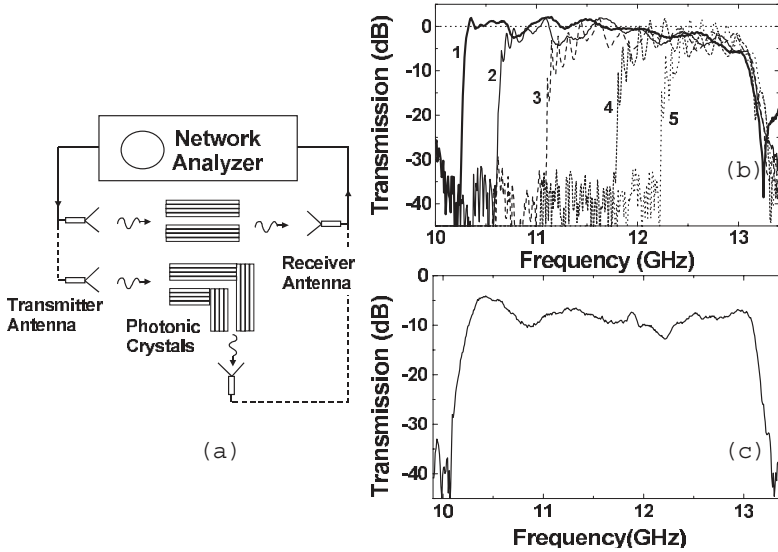
Figure 2. (a) Experimental set-up used to investigate the parallel-plate (upper case) and L-shaped (lower case) waveguide structures. (b) Transmission amplitude is measured from parallel-plate waveguides as the separation width of the waveguide is changed. The numbers given in the plot are assigned to width of the guides as (1) 18, (2) 16, (3) 14, (4) 12, and (5) 10.5 mm. (c) Transmission characteristics of the L-shaped waveguide.

stacking direction with a separation width, d, between them, while keeping a mirror type of symmetry between the rods of the two crystals [see Fig. 2(a)]. For the planar defect structure we have investigated in the first two sections, the propagation direction of the EM wave was perpendicular to the plane of the cavity. If the propagation direction is chosen to be parallel to the plane of the cavity, the structure will have the geometry of a parallel-plate waveguide. We expect the wave to be guided through the introduced air gap, starting from a cut-off frequency which depends on th ewidth of the gap. The guiding is limited with the full band gap frequency range of the photonic crystal, for which the crystal has the property of reflecting the EM waves in all directions.

We tested this waveguiding argument by measuring the transmission properties of these structures along the plane of the cavity. Figure 2(b) shows the transmission properties fo the waveguide structure for different separation widths. We observed full transmission

(100%) of the EM waves along a certain frequency range. The waveguiding was first observed at a minimum separation width around 10 mm, and the cut-off shifted to lower frequency values as the width of the air gap was increased. Independent of the width of the cavity, the guiding was observed to vanish at a fixed upper cut-off frequency (13.2 GHz), which correponds to the upper band-edge of the photonic band gap. This was along our expectations as the crystals do not act as mirrors (in all directions) beyond the full band gap frequencies. The lower cut-off frequency was determined by the width of the cavity and corresponds to the resonant frequency of the Fabry-Perot resonator. This resonant frequency can easily be predicted by a Fabry-Perot defect model we have used in our earlier work [6].

As we have pointed earlier, photonic crystal-based waveguides were predicted to have the property of guiding the wave through sharp bends [26]. To demonstrate this effect, we constructed an L-shaped waveguide in the following manner. We coupled the output of the previously described planar waveguide structure, to the input of another but identical waveguide making 90° with the first one, as shown in the second configuration of the set-up [see Fig. 2(a)]. Each wall of the waveguide is a 2-unit cell photonic crystal. The width of the cavity is kept at a value of 2 cm, for which the frequency range of the waveguide will overlap with the full banc gap of the crystals. Figure 2(c) shows the transmission of the EM waves through the L-shaped waveguide. The maximum magnitude of the transmitted signal was 35% of the incident signal. The frequency range of the L-shaped waveguide again covers the full band gap frequencies of the photonic crystal. These results show that photonic crystals can be used for various waveguide configurations.

We investigated the dispersion characteristics of the planar waveguide by measuring the phase difference of the transmitted wave introduced by the guide. This phase difference, ϕ_{trans}, can be written as $\phi_{\text{trans}} = kL - k_z L$, where $k = 2\pi f/c$ is the free space wavevector, k_z is the component of the wavevector along the waveguide [see Fig. 3(a)], and L is the length of the waveguide. This can be used to find the normalized propagation constant, k_z/k, as a function of frequency,

$$\frac{k_z}{k} = 1 - \frac{\phi_{\text{trans}}}{kL} = 1 - \frac{\phi_{\text{trans}}c}{2\pi f L}. \tag{1}$$

The dispersion relation calculated by this phase-measurement method is shown in Fig. 3(b) (solid lines) for different separation widths of the waveguide. The separation widths are chosen to be the same as those widths used in the transmission measurements given in Fig. 2(c).

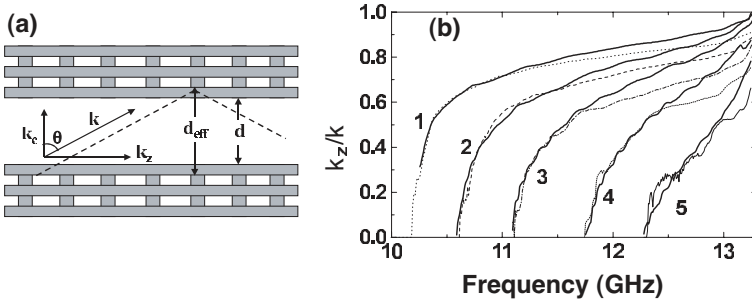The dispersion relations can also be calculated by a parallel-plate

Figure 3. (a) The vector diagram of the wave vector for the propagating wave inside the photonic crystal based waveguid. (b) Comparison of predicted (solid lines) and theoretically calculated (dotted lines) dispersion diagrams for the waveguides with different separation widths [see Fig. 2(b)].

waveguide model. Since the dielectric photonic crystal walls of the waveguide have a certain penetraion depth that can be calculated using the reflection-phase information from the walls of the cavity, we can define an effective width for the waveguide. This approach was previously used to investigate the defect characteristics built around dielectric and metallic photonic crystals [6]. In the calculation of this effective penetration depth, one must consider the angle dependence of the reflection phase, since the wave is considered to be bouncing between the walls of the waveguide at different angles for different frequencies. We measured the reflection phase of the EM waves from the walls of the cavity for the frequency range of the band gap, as a function of angle θ, where θ is taken to be the angle between the wavevector k and its component along the stacking direction of the crystal k_c as shown in Fig. 3(a). We calculated the effective width of the waveguide using the total phase contributions of both walls of the cavity, $\phi_{\mathrm{ref}}(\theta, f)$,

$$d_{\mathrm{eff}} = d + \frac{\phi_{\mathrm{ref}}(\theta, f)}{2k}, \qquad (2)$$

where d is the actual separation width of the waveguide. The corresponding propagation angle for each frequency is obtained from Eq. (1) as,

$$\theta = \arcsin\left(\frac{k_z}{k}\right) = \arcsin\left(1 - \frac{\phi_{\mathrm{trans}}c}{2\pi f L}\right). \qquad (3)$$

This angle information can be used in Eq. (2) to find an effective width of the guide at each frequency. The k_c component of the wavevector can

be calculated as $k_c = 2\pi/\lambda_c$, where $\lambda_c = 2d_{\text{eff}}$ is the cut-off wavelength of the waveguide. The dispersion relation can now be expressed as

$$\frac{k_z}{k} = \frac{\sqrt{k^2 - k_c^2}}{k}. \tag{4}$$

Note that since k_c is considered to be constant, after some frequency the square-root becomes real, so that the waves after that cut-off frequency (defined by k_c) can propagate in the guide. For frequencies less than the cut-off frequency, k_z is imaginary, and such modes (evanescent modes) cannot propagate in the waveguide [34]. Figure 3(b) compares the parallel-plate waveguide model dispersion relations [obtained from Eq. (4), dotted lines] with the dispersion relations obtained from the transmission phase measurements [using Eq. (1), solid lines]. As can be seen from the plots, the results are in good agreement for different separation widths of the guide, except for the higher frequency regions of the waveguide. This discrepancy is mainly related to the inaccurate reflection phase information (due to experimental limitations) at higher incidence angles, $\theta > 70°$.

3.2. Coupled-Cavity Waveguides (CCWs)

Recently, we have reported the eigenmode splitting, formation of bonding and antibonding modes (analagous to the electronic states in the diatomic molecules), due to the coupling of the evanescent modes in three-dimensional (3D) photonic crystals. Moreover, a transition from the discrete atomic-like states to the continuous spectrum (formation of a photonic band) was observed while increasing the number of defect cavities [18]. Although the modes of each cavity were tightly confined at the defect sites, overlap between the nearest-neighbor modes is enough to provide the propagation of photons via hopping [Fig. 4(a)]. This picture can be considered as the classical wave analog of the tight-binding (TB) method in solid state physics [18, 35–38].

In this section, we demonstrated the observation of guiding [Fig. 4(b)] and bending [Fig. 4(c)] of the EM wave through highly localized defect modes in a 3D photonic crystal [19]. The most important feature of these coupled cavity waveguides (CCW) is the possibility of constructing lossless and reflectionless bends. This ability has a crucial role to overcome the problem of guiding light around very sharp corners in the optical circuits.

We first measured the transmission characteristics of a straight waveguide which consists of 11 unit cell fct crystal. The defect array was created by removing a single rod from the first layer of each unit cell with a periodicity of $\Lambda = 1.28$ cm (see Fig. 5). A defect band
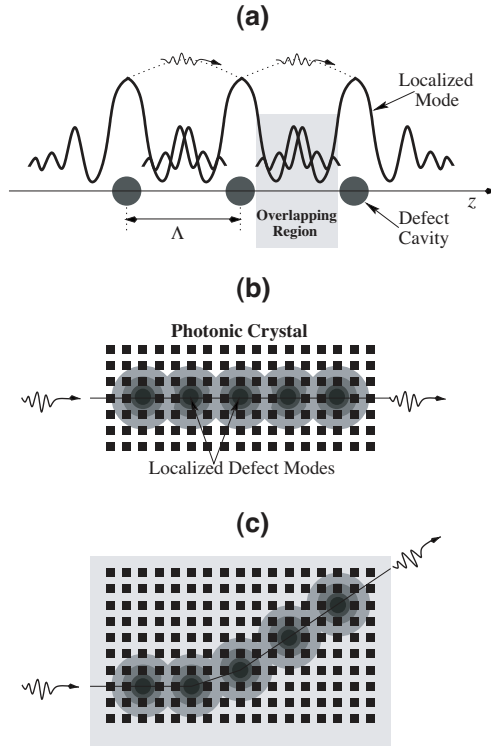
(a)

(b)

(c)

Figure 4. (a) Schematics of propagation of photons by hopping between the coupled evanescent defect modes. The overlap of the defect modes is large enough to provide propagation of the EM waves along tightly confined cavity modes. (b) A mechanism to guide light through localized defect modes in photonic crystals. (c) Bending of the EM waves around sharp corners.

(guiding band) was formed within the photonic band gap analagous to the impurity bands in the disordered semiconductors [Fig. 6(a)].

The width of this guiding band can be adjusted by changing the coupling strength between the cavities (for instance, the coupling increases when the distance between adjacent defects decreases). For this waveguide structure, nearly a complete transmission of the EM wave was observed within a frequency range extending from 11.47 to 12.62 GHz. It is interesting to note that when we placed one of the removed rods into its original position, we observed almost vanishing transmission amplitude throughout the above frequency range. This result is expected since the second nearest-neighbor coupling amplitude
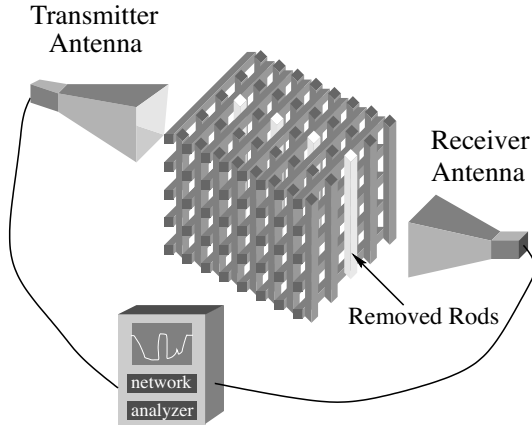
Figure 5. Experimental setup for measuring the transmission-amplitude and transmission-phase spectra of the coupled cavity waveguides (CCW) in layer-by-layer 3D photonic crystals.

is negligibly small in our structures.

To develop an optical circuit, the problem of the guiding light around sharp corners must be addressed. Conventional dielectric or metallic waveguides have large scattering losses when sharp bends are introduced. In order to test the bending of the EM wave around a sharp corner, we constructed a zig-zag shaped waveguide while keeping the distance between the consecutive cavities constant. In this waveguide, the propagation direction of photons was randomly changed. As shown in Fig. 6(b), we observed full transmission similar to the results obtained from the straight waveguide. Our results clearly indicate that the sharp corners have no influence on the propagation of EM waves in CCWs. By using CCWs one can achieve the bending of light around a sharp corner without any radiation losses. Therefore, this novel method may have great practical importance in certain applications.

The dispersion relation of the waveguiding band can be obtained from the transmission-phase measurements [39, 22]. By using the net phase difference $\delta\varphi$ between the phase of the EM wave propagating through the photonic crystal and the phase of the EM wave propagating in free space for a total crystal thickness L, one can determine the wave vector k of the crystal at each frequency from

$$k = \delta\varphi/L + 2\pi f/c, \tag{5}$$

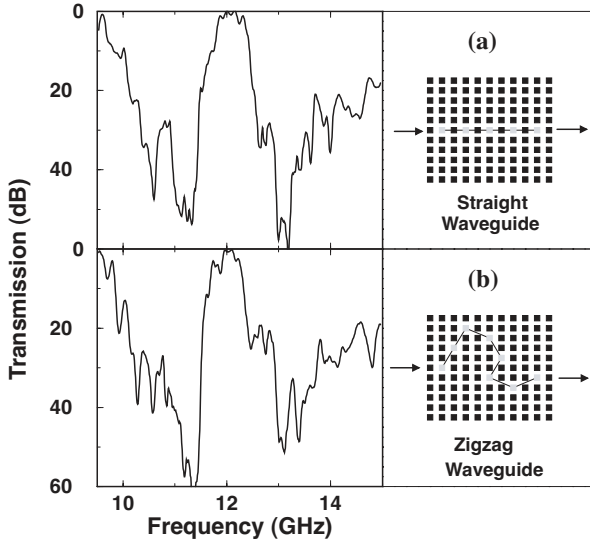where f is the frequency of the EM wave and c is the speed of the

Figure 6. (a) Transmission amplitude as a function of frequency for a straight waveguide geometry which is shown in the right panel. The gray squares represent the missing rods. A full transmission was observed throughout the entire waveguiding band ranging from 11.47 to 12.62 GHz. (b) Transmission characteristics of a zig-zag shaped waveguide which is formed by removing randomly chosen rods while keeping the distance between adjacent defects constant. In both cases, nearly 100 percent transmission amplitudes were measured.

light. The dispersion relation can also be determined within the TB approximation [35, 38, 18]

$$\omega_k \simeq \Omega[1 + \kappa \cos(k\Lambda)], \tag{6}$$

where $\Omega = 12.15$ GHz is the resonance frequency of a single defect, $\kappa = -0.047$ is a TB parameter which was experimentally determined from the splitting of two coupled cavities [18], and Λ is the distance between two consecutive defects.

We obtained the theoretical and experimental dispersion relations of the zig-zag shaped CCW by using Eq. (6) and the transmission-phase measurements. Figure 7(a) shows the comparison of measured and calculated dispersion relations. There is a good agreement between experiment and theory. In spite of the fact that the propagation direction of EM waves changed arbitrarily, nearly the same straight waveguide dispersion was obtained [18].
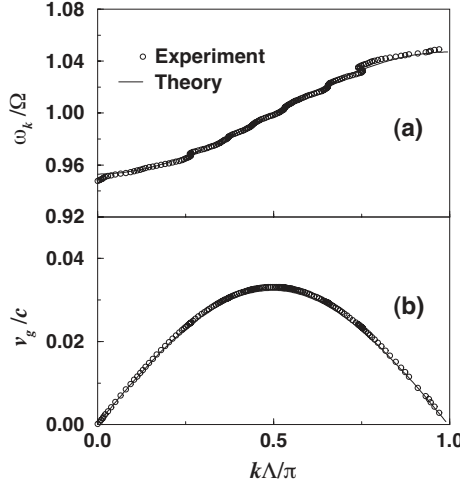
Figure 7. (a) The dispersion relation of the waveguiding band for the zig-zag shaped CCW. Experimental curve was obtained from the transmission-phase measurements via Eq. (5). (b) Group velocity v_g as a function of wave vector k. The measurements are in good agreement with the tight-binding predictions.

Group velocity of photons along the waveguide can be deduced from

$$v_g(k) = \nabla_k \omega_k = -\kappa \Lambda \Omega \sin(k\Lambda). \qquad (7)$$

Figure 7(b) displays the normalized group velocity as a function of wave vector k. Experimental group velocity was obtained from derivative of the best fitted function to the dispersion data. It is important to note that v_g vanishes at the band edges and the maximum group velocity is two orders of magnitude smaller than the speed of light. The small group velocity plays a critical role in the nonlinear optical processes. For example, sum-frequency generation can be enhanced at the band edges. In addition, the small group velocity leads to enhancement of the stimulated emission since the effective gain is proportional to $1/v_g$ [40].

The guiding or bending of EM waves through the localized defect modes via hopping is fundamentally different from previously proposed photonic crystal waveguides. Although, the structural imperfections such as misalignment of rods during the fabrication process affected the efficiency of the CCWs, we have observed nearly 100 percent transmission for various CCWs throughout the entire waveguiding band.

4. RESONANT CAVITY ENHANCED (RCE) DETECTORS

Defect structures built around the crystal were tested by putting them in the beam-path of the EM waves propagating along the stacking direction. A square law microwave detector was placed inside the defect volume of the photonic crystal, along with a monopole antenna. The monopole antenna was kept parallel to the polarization vector **e** of the incident EM wave in all measurements. The DC voltage on the microwave detector was used to measure the power of the EM field within the cavity. We also measured the enhanced field by feeding the output of the monopole antenna into the input port of the network analyzer. The monopole antenna was constructed by removing the shield around one end of a microwave coaxial cable. The exposed center conductor, which also acted as the receiver, was 2 mm long. The calibrated enhancement measurements were performed in the following manner. We first measured the enhanced EM field by the probe inside the cavity. While keeping the position of the probe fixed, we removed the crystal and repeated the smae measurement. This single pass absorption data of the probe was then used for calibration of the first measurement.

We first investigated the planar defect structure described in the previous section. Figure 8(a) shows the enhancement characteristics of this defect structure with a separation width of 8.5 mm. The measurement was done by the network analyzer and the frequency was chosen to cover the photonic band gap of our crystal. We observed a power enhancement factor of 1600 at a defect frequency of 11.68 GHz with a Q-factor 900. We then measured the enhancement characteristics of the same defect structure, with a microwave detector inserted inside the same cavity. An enhancement factor of 450 along with a Q-factor of 1100 was observed at the same defect frequency [Fig. 8(b), solid line].

The discrepancy between two measured enhancement factors can be explained by modeling our structure as a Fabry-Perot cavity. The crystals on each side of the cavity are considered as photonic mirrors of the Fabry-Perot cavity. The probe we used in our experiments was simulated by an absorption region of thickness l, with a relative absorption coefficient (α). We can write the power enhancement factor η, which is defined as the ratio of the stored power inside the absorption layer, to the incident EM wave, for the absorption region within the Fabry-Perot cavity,

$$\eta = \frac{(1 + R_2 e^{-\alpha l})(1 - R_1)}{1 - 2\sqrt{R_1 R_2} e^{-\alpha l} \cos(2\beta d + \phi_1 + \phi_2) + R_1 R_2 e^{-2\alpha l}}, \qquad (8)$$
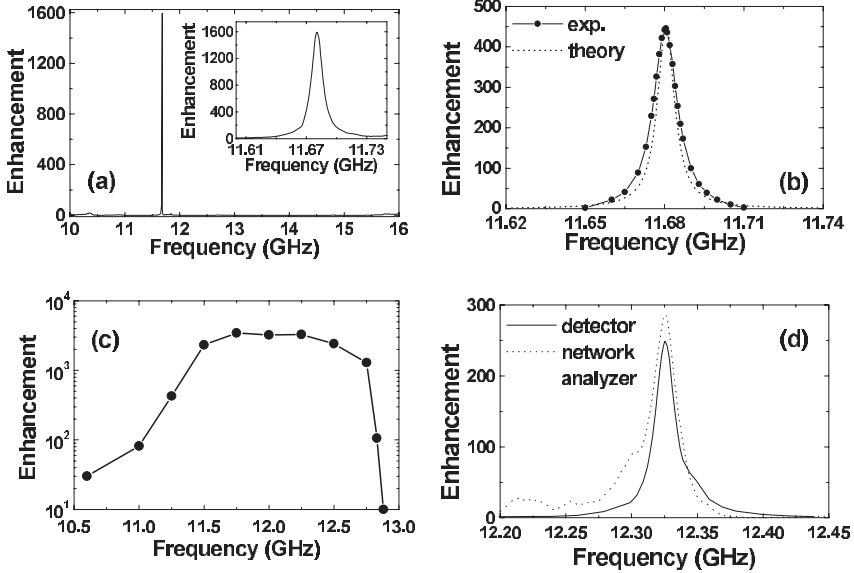
Figure 8. (a) Experimental enhancement factors obtained for a planar defect structure using the network analyzer. (b) Comparison of the experimental (solid line) and theoretical (dotted line) enhancement factors obtained for the RCE detector in the planar defect structure. (c) The power enhancement can be obtained at different resonant frequencies by changing the cavity width. This corresponds to a tuning band-width ranging from 10.5 to 12.8 GHz. (d) Enhancement characteristics of the box-like cavity measured by the network analyzer (dotted line) and the microwave detector (solid line).

where R_1 and R_2 are the reflectivities, ϕ_1 and ϕ_2 are the reflection phases of the mirrors of the cavity, β is the propagation constant of the EM wave in air, and d is the separation width of the cavity.

The above result is normalized with respect to the incident field absorbed by the detector in the absence of the crystal. The aforementioned planar defect structure has symmetric mirrors where $R = R_1 = R_2$. We used the measured transmission characteristics to obtain the reflectivities of our photonic mirrors. The rods were made of high quality alumina with a very low absorption coefficient, thus the absorption in the crystal can be neglected [23]. At the defect frequency, the tranmsission of an 8-layer crystal was 30 dB below the incident EM wave. The reflectivity of the photonic mirrors was then obtained as $R = 1 - T = 0.999$. The ideal case which maximizes η corresponds to $\alpha l = 0$, which gives a maximum enhancement

factor of 2000. We then varied αl to obtain enhancement factors closer to our experimental measurements. For $\alpha l = 0.0001$, Eq. (8) yields an enhancement factor of 1600 (which corresponds to the value obtained from the network analyzer), while $\alpha l = 0.0011$ results in an enhancement factor of 450 (microwave detector). The increased absorption factor for the detector measurement can be explained by the relatively large volume size of the microwave detector compared to monopole antenna alone. Figure 8(b) compares the measured (solid line) and simulated (dotted line) enhancements obtained for the RCE microwave detector within the planar defect structure. The theoretical Q-factor (1500) is comparable with the experimental Q-factor (1100).

The Fabry-Perot model suggests that η is maximized for the matching case $R_1 = R_2 e^{-2\alpha l}$ [41]. To increase the enhancement, we increased R_2 by adding one more unit cell (4 layers) to the mirror at the back. This resulted in an asymmetric planar cavity with a 2-unit cell thick front mirror, and a 3-unit cell thick back mirror. By varying the width of the planar cavity, we measured the enhancement factors at different resonant frequencies. As shown in Fig. 8(c), the tuning bandwidth of the RCE detector extends from 10.5 to 12.8 GHz. This tuning bandwidth of the RCE detector is in good agreement with the full photonic band gap (10.6–12.7 GHz) of the crystal [21]. As expected, the measured enhancement factors are relatively higher when compared with the symmetrical defect case. The maximum enhancement was measured as 3450 at a defect frequency of 11.75 GHz. The theory predicted enhancement factors around 5500, which is higher than the measured values. The discrepancy can be explained by the finite size of the photonic crystal, which limits the power enhancement of the field within the cavity.

In order to obtain a defect that is localized in three dimensions, we modified a 16-layer crystal structure in the following manner. Part of the rods on the 8th and 9th layers were removed to obtain a rectangular prism-like cavity. The dimensions of the cavity were $4a \times 4a \times 2t$, where $a = 1.12$ cm was the center-to-center distance between parallel rods, and $t = 0.32$ cm was the thickness of the alumina rods. We measured the power enhancement characteristics of this structure using the method described earlier. Figure 8(d) (dotted line) shows the measurement made by the network analyzer. An enhancement factor 290, and a Q-factor of 540 were measured at a defect frequency of 12.32 GHz. We then used a microwave detector within the cavity to probe the EM field inside the localized defect. As shown in Figure 8(d) (solid line), the maximum enhancement (245) occurred at the same frequency, along with a Q-factor of 680. Both measurements clearly indicate the resonant cavity enhancment for the localized defect.

5. HIGHLY DIRECTIONAL RESONANT ANTENNAS

Among the most important applications of photonic crystals, there is a great deal of growing interest for photonic crystal-based antennas [42, 43]. In microwave and millimeter-wave integrated circuits, the control of the radiation from a dipole antenna is of great importance. In such circuits, the antenna is mounted on a semiconductor substrate, which enhances the performance and functionality of the circuit. But most of the power from the antenna on a dielectric substrate is radiated into the substrate. Standard antennas on GaAs or Si radiate only 2–3% of their power into the air. If a thin substrate is used to overcome the loss due to this trapping, another problem arises. A 180° phase shift comes from the reflection at the bottom conductor, causing the radiation to cancel out at driving point. These problems can be solved, if the antenna is mounted on a 3-D photonic crystal, from which the radiation will fully be reflected in all directions.

The reported experimental and theoretical studies on the antenna applications mostly made use of the total reflection property of photonic crystals. The antennas mounted on photonic crystal substrate surfaces exhibited high efficiency and directivity compared to conventional antennas on dielectric substrates [44, 45]. Although high directivities which could be achieved using array antennas on photonic crystals were suggested [46], the maximum directivity that was demonstrated by Brown and McMahon using a photonic crystal-based single dipole antenna was 10, along with a radiative gain of 8 [44]. Very recently, a higher gain around 80 was reported using a 2-D photonic crystal cavity and a metallic mirror [47].

In this section, we report a photonic crystal-based resonant antenna with a very high directivity and gain. The antenna was formed by a hybrid combination of a monopole radiation source and a cavity built around layer-by-layer photonic crystal [8].

We used the output port of a microwave network analyzer and a monopole antenna to obtain EM waves. The monopole antennas as in the previous section was constructed by removing the shield around one end of a microwave coaxial cable. The cleaved center conductor, which also acted as the radiation source this time, was 6 mm long. An input port of the network analyzer and a standard gain horn antenna were used to receive the radiated EM field from the monopole antenna. The receiver was kept free to rotate around the crystal as shown in Fig. 9. The distance between the receiver and the crystal was around 50 cm.

We investigated the radiation characteristics of this monopole antenna, which was inserted into the planar defect structures built around a photonic crystal that consisted of 20 layers. The planar defect
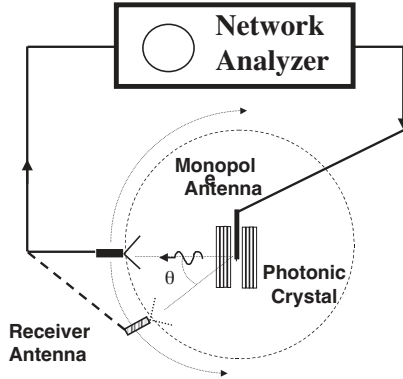
Figure 9. Experimental setup for measuring the radiation patterns of the monople antenna at various angles.

was formed by separating the 8th and 9th layers of the structure, as described in the previous section. In order to suppress the radiation in the backward direction, we intentionally chose one of the crystals of the cavity to have a higher reflectivity than the front crystal. This resulted in an asymmetric planar cavity with a two unit-cell (8 layers) front crystal, and a three-unit cell (12 layers) back crystal. The intensity through the back crystal is $\sim$ 18–20 dB lower than the front crystal in the $0°$ direction. If a symmetric cavity was used, two directional beams would emerge in both directions.

In the H-plane measurements, the antenna and the polarization axis of the receiver horn antenna were kept vertical and were parallel to each other at all incidence angles. We then rotated the antenna, photonic crystal and the horn antenna 90 degrees (so that the monopole antenna and the polarization axis of the horn were horizontal) to measure the radiation pattern in the perpendicular plane (E-plane). In all these measurements, the monopole antenna was kept close to the back crystal of the cavity. The antenna was parallel to the surface rods of the back crystal to maximize the directivity and the detected power.

Antenna radiation patterns were simulated with the widely used finite-difference-time-domain (FDTD) technique [43]. To reduce the FDTD computational space, a short dipole antenna was used in the simulations which should approximate well the monopole antenna. The time-dependent Maxwell's equations were numerically integrated with the fixed frequency dipole source inside the defect volume of the photonic crystal, to obtain the far-field radiation pattern. The calculations were repeated at different frequencies of the dipole source.
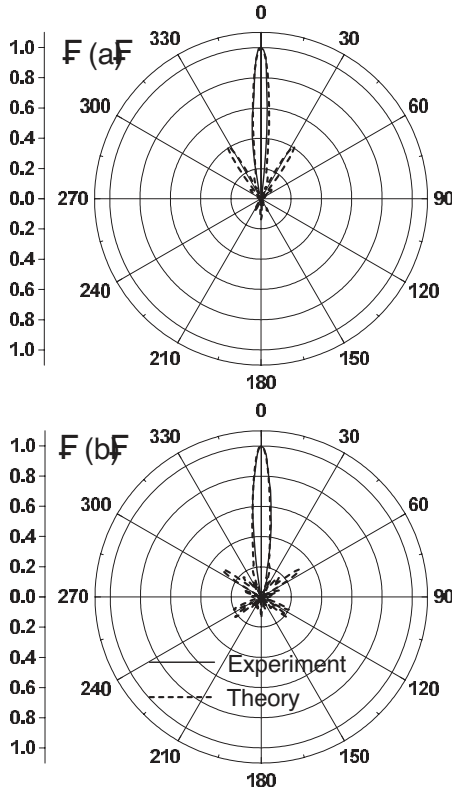
Figure 10. The measured (solid lines) and calculated (dotted lines) radiation patterns of the monopole antenna inside the cavity of the photonic crystal for (a) H-field and (b) E-field. The measurements and simulations were made at the resonance frequency of 11.7 GHz.

We first measured the detected power at the resonance frequency of the cavity as a function of angle. Figure 10(a) (solid line) shows the normalized radiation pattern in H-plane, which was measured at the resonance frequency of the cavity. We observed a strong radiation around $\theta = 0°$, where the radiation along other directions is highly suppressed. The measurements performed in the other plane [E-plane, Fig. 10(b), solid line] also resulted in similar radiation pattern. The measured (solid lines) and calculated (dotted lines) radiation patterns for both planes agree well. The simulations also predict a directed radiation pattern that displays the same trends but has side lobes other than the major lobe. We also observed such radiations along similar angles in the experiment, but we were able to suppress them by slightly

varying the position of the monopole antenna within the cavity. We repeated these measurements with antennas having different lengths, and we observed no significant change in the radiation patterns for both planes.

For antennas with one narrow major lobe and negligible minor lobes in the radiation pattern, the maximum directivity is approximately equal to [48]

$$D_0 \simeq \frac{4\pi}{\Theta_1 \Theta_2}, \tag{9}$$

where Θ_1 is the half-power beamwidth in one plane and Θ_2 in the perpendicular plane to the first, in radians. The measured half-power beamwidth along the H-plane [Fig. 10(a)] was 12 degrees, and was 11 degrees along the E-plane [Fig. 10(b)]. These values lead to a directivity value around 310.

Figure 11(a) (solid line) shows the detected microwave power as a function of frequency at $\theta = 0°$. The dotted line displays the detected microwave power at the same angle in the absence of the photonic crystal. The ratio between these two measurements is defined as the power enhancement factor due to the presence of the photonic crystal. At resonance frequency, we observed a power enhancement factor of 180 (22.6 dB) at a defect frequency of 11.725 GHz. The radiated EM field from the monopole antenna has also frequency selectivity introduced by the cavity. The Q factor was measured to be 895.

In order to understand the effect of the resonator to the efficiency of the monopole antenna, we also measured the S-parameters of our antenna structure. Figure 11(b) shows the reflection power coefficient (S11) which is 30% (-5 dB) for the monopole antenna standing alone in air. This implies that the antenna radiates only 70% of the incoming power. When the antenna was inserted inside the cavity, we observed a very sharp drop (-35 dB) at resonance frequency in the reflection spectra [Fig. 11(b), solid line]. This drop indicates that most of the power (99.7%) is radiated out in the presence of the cavity. The maximum radiation gain for our antenna is related to the maximum directivity by $G_0 = (1 - R)(1 - A)D_0$, where R is the reflected power and A is the absorptivity of the antenna. In our case, the reflectivity at the resonance frequency is very small (0.0003). Assuming that the absorption in the antenna has a negligible value, the maximum gain has a value around 300.

Such a planar cavity built around a 3-D photonic crystal should not be confused with the Fabry-Perot type of resonators that are constructed by using distributed Bragg reflectors (which are known as 1-D photonic crystals). In the former structure, the EM field is always coupled to the evanescent defect mode within the band gap
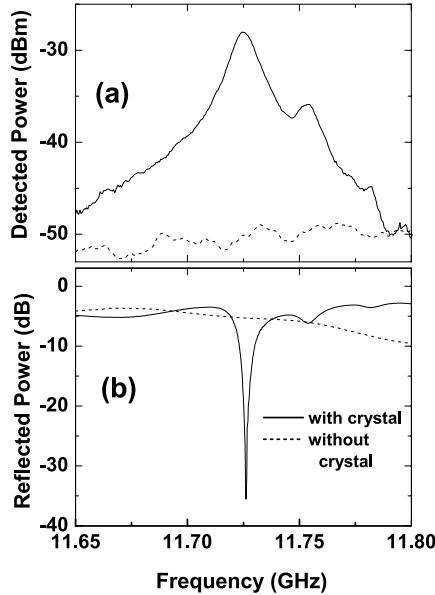
Figure 11. (a) Detected power of the monopole antenna with (solid line) and without (dashed line) photonic crystal around resonance frequency at $\theta = 0°$. (b) The reflection power coefficient (S11) measured with (solid line) and without (dashed line) photonic crystal.

irrespective of the incidence angle. However, the resonant frequency shifts as the angle of incidence of the EM wave changes in the latter case [48, 49]. It is obvious that for planar waves, 3-D and 1-D resonant structures will result in similar enhancements and directivities. In our case, the monopole antenna radiates in all directions, and all the power radiated is coupled to the evanescent mode of the defect, regardless of the direction. This is the reason we have an antenna with a very high efficiency [see Fig. 11(b)]. However, for a 1-D structure, the radiated EM field, except a certain direction, will not be coupled to the corresponding resonant mode of the cavity.

Although our structure is suitable for narrow bandwidth applications, one can tune the defect frequency to any desired value by adjusting the width of the cavity. We observed that the resonance frequency could be tuned within a frequency range extending from 10.6 to 12.8 GHz, which corresponds to the full band gap of our photonic crystal. The directivity drops to values around 100 at the band edges, and reaches a peak value of 310 at 11.7 GHz.

6. SUMMARY

In this paper, we have demonstrated three different applications of the layer-by-layer 3D photonic crystals at microwave frequencies. The first application is the guidance of the EM waves with 100% transmission, using photonic crystals. We have developed a parallel-plate waveguide model for our structures. The dispersion diagrams calculated using the transmitted phase measurements and by the waveguide model were in good agreement. Moreover, we have demonstrated a new mechanism to manipulate propagation of EM waves in 3D photonic crystals. Photons hop from one evanescent defect mode to the next one, regardless of the direction of propagation. A complete (near 100 percent) transmission of the EM wave along a straight path and around sharp corners were observed experimentally. The measured dispersion relation of the waveguiding band agreed well with the results of the classical wave analog of the tight-binding method.

Second, we suggest the possibility of using an embedded detector inside the crystal, as an RCE detector. By using smaller size photonic crystals and higher frequency detectors, the RCE effect can also be obtained at millimeter and far-infrared frequencies. These frequency selective RCE detectors have increased sensitivity and efficiency when compared to conventional detectors, and can be used for various applications. In the third application, we used the hybrid combination of a monopole radiation source and a cavity built around photonic crystals. This combination exhibited a highly directional and enhancement radiation source. Since the Maxwell's equations have no fundamental length scale, our microwave results can be extended to the optical frequencies.

REFERENCES

1. Yablonovitch, E., "Inhibited spontaneous emission in solid-state physics and electronics," *Phys. Rev. Lett.*, Vol. 58, 2059, 1987.
2. John, S., "Strong localization of photons in certain disordered dielectric superlattices," *Phys. Rev. Lett.*, Vol. 58, 2486, 1987.
3. Joannopoulos, J. D., R. D. Meade, and J. N. Winn, *Photonic*

Crystals: Molding the Flow of Light, Princeton University Press, Princeton, NJ, 1995.

4. For a recent review, see articles in , *Photonic Crystals and Light Localization in the 21st Century*, C. M. Soukoulis (ed.), Kluwer, Dortrecht, 2001.

5. Wanke, M. C., O. Lehmann, K. Muller, Q. Wen, and M. Stuke, "Laser rapid prototyping of photonic band-gap microstructures," *Science*, Vol. 275, 1284, 1997.

6. Temelkuran, B., E. Ozbay, J. P. Kavanaugh, G. Tuttle, and K. M. Ho, "Resonant cavity enhanced detectors embedded in photonic crystals," *Appl. Phys. Lett.*, Vol. 72, 2376, 1998.

7. Temelkuran, B. and E. Ozbay, "Experimental demonstration of photonic crystal based waveguides," *Appl. Phys. Lett.*, Vol. 74, 486, 1999.

8. Temelkuran, B., M. Bayindir, E. Ozbay, R. Biswas, M. M. Sigalas, G. Tuttle, and K. M. Ho, "Photonic crystal based resonant antenna with a very high directivity," *J. Appl. Phys.*, Vol. 87, 603, 2000.

9. Lin, S. Y., J. G. Fleming, D. L. Hetherington, B. K. Smith, R. Biswas, K. M. Ho, M. M. Sigalas, W. Zubrzycki, S. R. Kurtz, and J. Bur, "A three-dimensional photonic crystal operating at infrared wavelength," *Nature* (London), Vol. 394, 251, 1998.

10. Fleming, J. G. and S.-Y. Lin, "Three-dimensional photonic crystal with a stop band from 1.35 to 1.95 μm," *Opt. Lett.*, Vol. 24, 49, 1999.

11. Noda, S., K. Tomoda, N. Yamamoto, and A. Chutinan, "Full three-dimensional photonic bandgap crystals at near-infrared wavelengths," *Science*, Vol. 289, 604, 2000.

12. Villeneuve, P. R., S. Fan, J. D. Joannopoulos, K.-Y. Lim, G. S. Petrich, L. A. Kolodziejski, and R. Reif, "Air-bridge microcavities," *Appl. Phys. Lett.*, Vol. 67, 167, 1995.

13. Gourley, P. L., J. R. Wendt, G. A. Vawter, T. M. Brennan, and B. E. Hammons, "Optical properties of two dimensional photonic lattices fabricated as honeycomb nanostructures in compound semiconductors," *Appl. Phys. Lett.*, Vol. 64, 687, 1994.

14. Dowling, J. P., M. Scalora, M. J. Bloemer, and C. M. Bowden, "The photonic band edge laser: a new approach to gain enhancement," *J. Appl. Phys.*, Vol. 75, 1896, 1994.

15. Yablonovitch, E., T. J. Gmitter, R. D. Meade, A. M. Rappe, K. D. Brommer, and J. D. Joannopoulos, "Donor and acceptor modes in photonic band structure," *Phys. Rev. Lett.*, Vol. 67, 3380,

1991.

16. Painter, O., R. K. Lee, A. Scherer, A. Yariv, J. D. O'Brien, P. D. Dapkus, and I. Kim, "Two-dimensional photonic band-gap defect mode laser," *Science*, Vol. 284, 5421, 1999.

17. Mekis, A., M. Meier, A. Dodabalapur, R. E. Slusher, and J. D. Jaonnopoulos, "Lasing mechanism in two-dimensional photonic crystal lasers," *Appl. Phys. A: Mater. Sci. Process*, Vol. 69, 111, 1999.

18. Bayindir, M., B. Temelkuran, and E. Ozbay, "Tight-binding description of the coupled defect modes in three-dimensional photonic crystals," *Phys. Rev. Lett.*, Vol. 84, 2140, 2000.

19. Bayindir, M., B. Temelkuran, and E. Ozbay, "Propagation of photons by hopping: a waveguiding mechanism through localized coupled-cavities in three-dimensional photonic crystals," *Phys. Rev. B*, Vol. 61, R11855, 2000.

20. Ho, K. M., C. T. Chan, C. M. Soukoulis, R. Biswas, and M. Sigalas, "Photonic band gaps in three dimensions: new layer-by-layer periodic structures," *Solid State Commun.*, Vol. 89, 413, 1994.

21. Ozbay, E., "Layer-by-layer photonic band gap crystals: from microwave to the far-infrared," *J. Opt. Soc. Am. B*, Vol. 13, 1945, 1996.

22. Ozbay, E., A. Abeyta, G. Tuttle, M. Tringides, R. Biswas, C. T. Chan, C. Soukoulis, and K. M. Ho, "Measurement of a three-dimensional photonic band gap in a crystal structure made of dielectric rods," *Phys. Rev. B*, Vol. 50, 1945, 1994.

23. Ozbay, E. and B. Temelkuran, "Reflection properties and defect formation in photonic crystals," *Appl. Phys. Lett.*, Vol. 69, 743, 1996.

24. Kosaka, H., T. Kawashima, A. Tomita, M. Notomi, T. Tamamura, T. Sato, and S. Kawakami, "Photonic crystals for micro light-wave circuits using wavelength-dependent angular beam steering," *Appl. Phys. Lett.*, Vol. 74, 1370, 1999.

25. de Lustrac, A., F. Gadot, S. Cabaret, J.-M. Lourtioz, T. Brillat, A. Priou, and E. Akmansoy, "Experimental demonstration of electrically controllable photonic crystals at centimenter wavelengths," *Appl. Phys. Lett.*, Vol. 75, 1625, 1999.

26. Mekis, A., J. C. Chen, I. Kurland, S. Fan, P. R. Velleneuve, and J. D. Joannopoulos, "Hight transmission through sharp bends in photonic crystal waveguides," *Phys. Rev. Lett.*, Vol. 77, 3787, 1996.

27. Lin, S.-Y., E. Chow, V. Hietala, P. R. Villeneuve, and J. D. Joannopoulos, "Experimental demonstration of guiding and bending of electromagnetic waves in a photonic crystal," *Science*, Vol. 282, 274, 1998.

28. Sigalas, M. M., R. Biswas, K. M. Ho, C. M. Soukoulis, D. Turner, B. Vasiliu, S. C. Kothari, and S. Lin, "Waveguide bends in three-dimensional layer-by-layer photonic bandgap materials," *Micro. Opt. Tech. Lett.*, Vol. 23, 56, 1999.

29. Baba, T., N. Fukaya, and J. Yonekura, "Observation of light propagation in photonic crystal optical waveguides with bends," *Electron. Lett.*, Vol. 35, 654, 1999.

30. Tokushima, M., H. Kosaka, A. Tomita, and H. Yamada, "Light-wave propagation through a 120° sharply bent single-line-defect photonic crystal waveguide," *Appl. Phys. Lett.*, Vol. 76, 952, 2000.

31. Loncar, M., D. Nedeljkovic, T. Doll, J. Vuckovic, A. Scherer, and T. P. Pearsall, "Waveguiding in planar photonic crystals," *Appl. Phys. Lett.*, Vol. 77, 1937, 2000.

32. Johnson, S. G., P. R. Villeneuve, S. Fan, and J. D. Joannopoulos, "Linear waveguides in photonic-crystal slabs," *Phys. Rev. B*, Vol. 62, 8212, 2000.

33. Noda, S., A. Chutinan, and M. Imada, "Trapping and emission of photons by a single defect in a photonic bandgap structure," *Nature* (London), Vol. 407, 608, 2000.

34. Jackson, J. D., *Classical Electrodynamics*, 2nd ed., Wiley, New York, 1975.

35. Stefanou, N. and A. Modinos, "Impurity bands in photonic insulators," *Phys. Rev. B*, Vol. 57, 12127, 1998.

36. de Sterke, C. M., "Superstructure gratings in the tight-binding approximation," *Phys. Rev. E*, Vol. 57, 3502, 1998.

37. Lidorikis, E., M. M. Sigalas, E. N. Economou, and C. M. Soukoulis, "Tight-binding parametrization for photonic band gap materials," *Phys. Rev. Lett.*, Vol. 81, 1405, 1998.

38. Yariv, A., Y. Xu, R. K. Lee, and A. Scherer, "Coupled-resonator optical waveguide: a proposal and analysis," *Opt. Lett.*, Vol. 24, No. 711, 1999; Y. Xu, R. K. Lee, and A. Yariv, "Propagation and second-harmonic generation of electromagnetic waves in a coupled-resonator optical waveguide," *J. Opt. Soc. Am. B*, Vol. 17, 387, 2000.

39. Robertson, W. M., G. Arjavalingam, R. D. Meade, K. D. Brommer, A. M. Rappe, and J. D. Joannopoulos, "Measurement of photonic band structure in a two-dimensional periodic dielectric

array," *Phys. Rev. Lett.*, Vol. 68, 2023, 1992.

40. Sakoda, K., "Enhanced light ampli cation due to group-velocity anomaly peculiar to two- and three-dimensional photonic crystals," *Opt. Express*, Vol. 4, 167, 1999.

41. Unlu, M. S. and S. Strite, "Resonant cavity enhanced photonic devices," *J. Appl. Phys.*, Vol. 78, 1995.

42. Brown, E. R., C. D. Parker, and E. Yablonovitch, "Radiation properties of a planar antenna on a photonic-crystal substrate," *J. Opt. Soc. Am. B*, Vol. 10, 404, 1993.

43. Sigalas, M. M., R. Biswas, Q. Li, D. Crouch, W. Leung, R. Jacobs-Woodbury, B. Lough, S. Nielsen, S. McCalmont, G. Tuttle, and K. M. Ho, "Dipole antennas on photonic bandgap crystals: experiment and simulation," *Micro. Opt. Tech. Lett.*, Vol. 15, 153, 1997.

44. Brown, E. R. and O. B. McMahon, "High zenithal directivity from a dipole antenna on a photonic crystal," *Appl. Phys. Lett.*, Vol. 68, 1300, 1996.

45. Gonzalo, R., P. de Maagt, and M. Sorolla, "Enhanced patch-antenna performance by suppressing surface waves using photonic-bandgap substrates," *IEEE Trans. Microwave Theory Tech.*, Vol. 47, 2131, 1999.

46. Poilasne, G., P. Pouliguen, K. Mahdjoubi, J. Lenormand, C. Terret, and Ph. Gelin, "Theoretical study of grating lobes reduction using metallic photonic bandgap materials (MPBG)," *Micro. Opt. Tech. Lett.*, Vol. 18, 32, 1998.

47. Thevenot, M., C. Cheype, A. Reineix, and B. Jecko, "Directive photonic-bandgap antennas," *IEEE Trans. Microwave Theory Tech.*, Vol. 47, 2115, 1999.

48. Yariv, A. and P. Yeh, *Optical Waves in Crystals*, Wiley, New York, 1984.

49. Schubert, E. F., N. E. J. Hunt, A. M. Vredenberg, T. D. Harris, J. M. Poate, D. C. Jacobson, Y. H. Wong, and G. J. Zydzik, "Increased fiber communications bandwidth from a resonant cavity light emitting diode emitting at $\lambda = 940\,\text{nm}$," *Appl. Phys. Lett.*, Vol. 63, 2603, 1993.